HYBRID SOFT SOIL TIRE MODEL (HSSTM).

PART I: TIRE MATERIAL AND STRUCTURE MODELING

Taheri, Sh.[a,1], Sandu, C.[a] , Taheri, S.[a], Gorsich, D.[b]

[a]*Department of Mechanical Engineering, Virginia Tech, Blacksburg, VA, USA*

[b]*U.S. Army TARDEC, MI, USA*

Abstract

In order to model the dynamic behavior of the tire on soft soil, a lumped mass discretized tire model using Kelvin-Voigt elements is developed. To optimize the computational time of the code, different techniques were used in memory allocation, parameter initialization, code sequence, and multi-processing. This has resulted in significant improvements in efficiency of the code that can now run close to real time and therefore it is suitable for use by commercially available vehicle simulation packages.

Model parameters are obtained using a validated finite element tire model, modal analysis, and other experimental test procedures. Experimental tests were performed on the Terramechanics rig at Virginia Tech. The tests were performed on different terrains (such as sandy loam) and tire force and moments, soil sinkage, and tire deformation data were collected for various case studies based on a design of experiment matrix. This data, in addition to modal analysis data were used to validate the tire model. Furthermore, to study the validity of the tire model, simulations at conditions similar to the test conditions were performed on a quarter car model. The results have indicated the superiority of this model as compared to other lumped parameter models currently available.

Keywords: Wheeled Vehicle, Terramechanics, Off-Road, Deformable Terrain, Tire Model, Soil, Parameterization, Mobility

[1]Corresponding author email address:
taheri@vt.edu

Report Documentation Page

Form Approved
OMB No. 0704-0188

1. REPORT DATE	2. REPORT TYPE	3. DATES COVERED
28 APR 2015		**00-00-2015 to 00-00-2015**

4. TITLE AND SUBTITLE	5a. CONTRACT NUMBER
Hybrid Soft Soil Tire Model (HSSTM) Part I: Tire Material and Structure Modeling	5b. GRANT NUMBER
	5c. PROGRAM ELEMENT NUMBER
6. AUTHOR(S)	5d. PROJECT NUMBER
	5e. TASK NUMBER
	5f. WORK UNIT NUMBER
7. PERFORMING ORGANIZATION NAME(S) AND ADDRESS(ES) **US Army RDECOM-TARDEC,6501 E. 11 Mile Road,Warren,MI,48397-5000**	8. PERFORMING ORGANIZATION REPORT NUMBER
9. SPONSORING/MONITORING AGENCY NAME(S) AND ADDRESS(ES)	10. SPONSOR/MONITOR'S ACRONYM(S)
	11. SPONSOR/MONITOR'S REPORT NUMBER(S)

12. DISTRIBUTION/AVAILABILITY STATEMENT
Approved for public release; distribution unlimited

13. SUPPLEMENTARY NOTES

14. ABSTRACT
See Report

15. SUBJECT TERMS

16. SECURITY CLASSIFICATION OF:			17. LIMITATION OF ABSTRACT	18. NUMBER OF PAGES	19a. NAME OF RESPONSIBLE PERSON
a. REPORT **unclassified**	b. ABSTRACT **unclassified**	c. THIS PAGE **unclassified**	**Same as Report (SAR)**	**40**	

1 Introduction

The tire forces and moments depend on the structural behavior of the tire, as well as tire-terrain interaction. Therefore, based on the simulation application (e.g., handling, ride, mobility, durability), and type of the terrain (e.g., deformable, non-deformable, even, uneven) the approach for modeling the tire and the terrain would be different. The tire models that are used for vehicle simulation on mainly non-deformable terrains, such as FTire [1], RMOD-K [2, 3], CDTire [4], can be categorized based on usage, accuracy, computational efficiency, and degree of parameterization. The number of degrees-of-freedom (DOFs) and consequently the computational effort in these models can be sorted from empirical models (lowest) to finite element models (highest).

A direct application of an on-road tire model to simulate tire performance on soft soil is not possible. This is due to the fact that traveling on deformable terrain raises issues for which on-road tire models do not account for. Moreover, the kinetics and kinematics of the tire on deformable terrains are subjected to different design and operational factors, as well as field characteristics. These factors, in addition to the uncertainties that exist in their parameterization, make the formulation of tire-terrain interaction a highly complex problem. Due to this complexity, the number of tire models, similar to the one developed in this research that are usable in conjunction with multibody dynamic vehicle simulation models, are limited.

The proposed process of developing the complete soft soil tire model can be divided into two main sub-processes of mathematical modeling and physical modeling, as shown in Figure 1. For the mathematical modeling, different components of the system, such as tire material, tire structure and tire-ground interaction are described using semi-empirical mathematical correlations. Next, these mathematical models are implemented using a programing language, such as MATLAB. The developed code is checked to confirm that the model is correctly implemented and is free of errors. Meanwhile, a physical representation of the problem is essential to provide an insightful look into the real world situation. In this regard, an experimental test rig is designed for conducting the related case studies. The type and configuration of these experiments, which are required for validating and parameterizing the implemented sub-models, are developed as a design of experiment table.

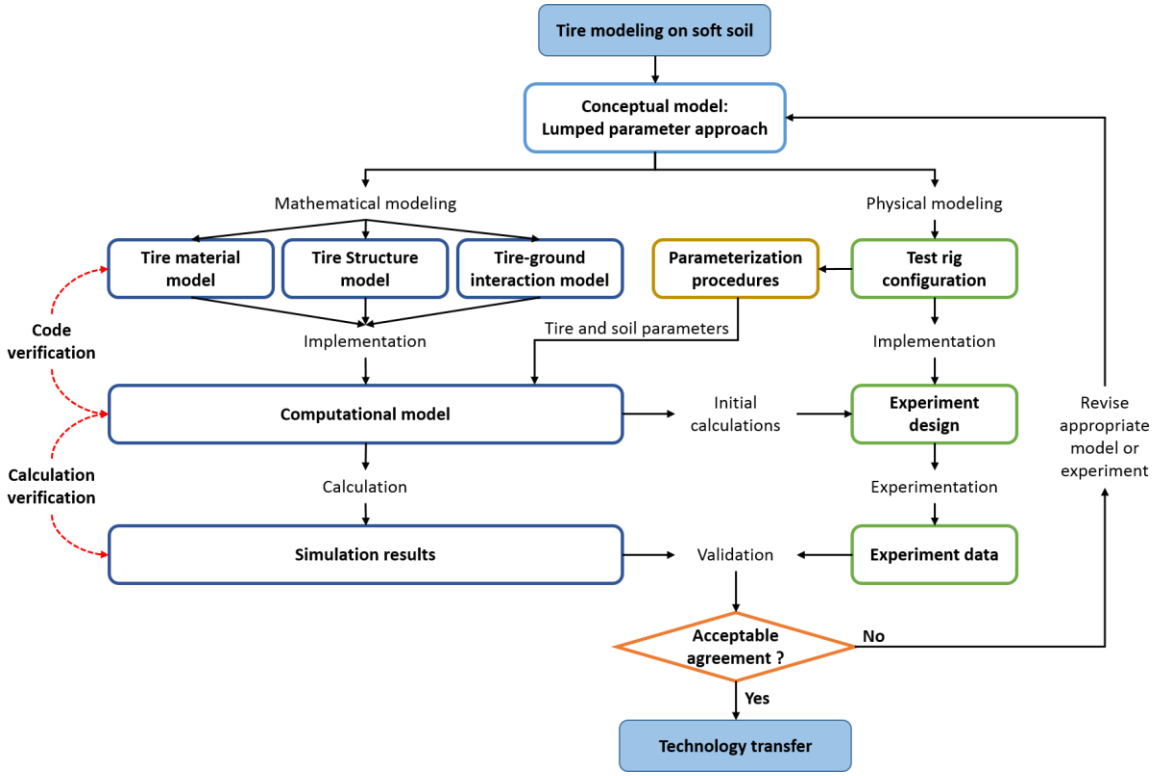

Figure. 1 - Tire modeling on the soft soil: Modeling, simulation, and experimental procedures work flow.

Using the parameters derived for the computational model, simulations are performed at conditions similar to the experiments. The results from this step are iteratively generated and compared to the test data until the acceptable agreement is achieved. In case the correlation accuracy was not achieved after extensive simulation iterations, the judgment is made whether to make changes to one of the sub-models, experimental setup, parameterization procedures, or all of the above. In the following sections, first a brief literature survey for the available tire models that are designed for estimating the tire performance on deformable surfaces is given. Next, steps that are required for accurately characterizing the tire structure behavior are elaborated in more details. It should be mentioned that the development of the tire-ground interaction model is discussed in a companion paper [5]. Representative simulation results for the newly developed tire model, called Hybrid Soft Soil Tire Model (HSSTM) are discussed.

2 Literature Survey

As mentioned earlier, the main challenge in studying the behavior of the vehicle in off-road condition is characterizing the tire-terrain interaction. Throughout the years, a wide variety of models have been developed for

formulating and simulating this interaction. The degree of complexity for these models is based on the application, accuracy, and computational cost. Generally, these models can be grouped into three main categories [6]: 1) Empirical models, 2) semi-empirical models, and 3) physics-based models. The literature survey included in this paper is brief, but the authors published an extensive review paper on this topic, and the reader is encouraged to refer to [6]

2.1 Empirical models

The empirical models use the experimental data of the tire response, and correlate it to the influential parameters of the system via mathematical equations. One of the most famous empirical models is the Magic Formula Tire Model, presented by Pacejka [7]. This model is based on the tire steady-state response data, and relates the tire forces and moments to wheel pure slip values

Empirical models are very useful as simple tools for evaluating the performance of the vehicles in conditions similar to the test environment and with tire properties similar to the test tire [2, 8-10]. Due to these limitations, empirical models cannot be used for extrapolating the results to the problems outside the scope of the specific experimental tests under which the data has been obtained. Thus, a new tire design concept or a new operating condition for testing the tire performance cannot be studied using this family of tire models. The empirical models developed for passenger and truck size tires do not scale perfectly to the smaller size tires, such as tires in robotic applications and planetary exploration vehicles. Furthermore, empirical tire models require several sets of data for their parameter estimation process that increases the cost of experimental procedure.

2.2 Physics based models

A tire on road is constantly excited by road unevenness with short and long wavelengths. Consequently, it operates as a filter over the road roughness. Capturing the tire-road interaction for road inputs with high frequency (short wavelengths), relative to the size of the contact patch, is more complex. The tire response at the spindle of the tire is usually smoother than the shape of the obstacle. This behavior has two main reasons; first, when the tire travels over an obstacle, such as a cleat, the forehead of the tire touches the obstacle before the wheel center. Therefore, the distance traveled by the tire while interacting with an obstacle is longer than the length of the obstacle. Second, the tire has some flexibility at its contact patch, which almost swallows the small irregularities during the enveloping process [11]. Capturing this filtering performance is the main motive for several physic-based tire models.

Physics based models incorporate the physical principles and analytical methods to represent tire and terrain structures in addition to their interaction [12]. This multi-disciplinary field of models incorporates applied mathematics, numerical analysis, computational physics, and even computer graphics to evaluate the performance of wheeled vehicles [13]. The degree of complexity varies from the simple models that consider tire as a rigid ring and terrain as a spring-damper system to very detailed models that use finite element formulation for both tire and terrain [14, 15].

2.3 Semi-empirical models

Mechanical behavior of the tire and tire-terrain depends on many aspects, such as tire geometrical and material properties, in addition to terrain texture and frictional characteristics. Identifying all of these parameters and correlating them to the vehicle performance using empirical closed-form formulations are limited to the similar test conditions. On the other hand, using the simple physics-based methods to model the terrain can lead to significant errors in both estimating model parameters and capturing terrain mechanics. This will ultimately cause the vehicle response to deviate from the experimental data. One alternative numerical method for analyzing vehicle performance is the semi-empirical models [16-19]. In this category of tire models, the tire structure is usually modeled by analytical equations and the terrain is defined using empirically derived models [20]. These models are best nominees for dynamic vehicle simulations because they are a trade-off between accuracy and computational efficiency [11-13].

The majority of the models in this field use the two-dimensional empirical formulation developed by Bekker and Wong [21-28]. In these formulations, the tire is commonly considered as a rigid cylinder, and the normal and shear stresses in the tire contact patch are expressed as functions of the tire kinetics and kinematic variables. Consequently, the corresponding stress components are integrated over the contact patch to calculate the spindle forces, tire sinkage, soil deformation, tire deflection, etc. The more sophisticated tire models use a finite element representation for either tire structure or tire-ground interaction.

The proposed tire model is considered as a semi-empirical tire model because it takes a physics-based lumped parameter approach for describing the tire structural response in addition to a semi-empirical method for characterizing the tire-terrain interaction.

3 Tire material modeling

A typical modern tire is manufactured from nearly 10-35 different components. Information about tire material properties, processing, mixing, assembly, and curing are almost always confidential, and cannot be received from tire companies. Furthermore, the material properties for the same tire from a manufacturer may vary, due to the vulcanization process, for example. In order to accurately estimate the behavior of the tire components, elaborate material models are needed. The parameterization of these models for individual materials in the tire requires performing extensive experimental and analytical procedures, such as elastic and viscoelastic tests on individual tire sections. This level of detail is required for calculating the accurate stress and strains in the tire structure, which would be helpful in the design stage of the tire.

The main scope of this study is to estimate the tire mobility performance factors including forces and moments at the tire spindle. Therefore, simplified methods are chosen for describing the tire material behavior, such as hyperelasticity and viscoelasticity.

3.1 Hyperelasticity

A great portion of the tire structure consists of vulcanized elastomers, such as rubber material. Rubber has a nonlinear and incompressible behavior toward loading, which is independent of the strain rate. This behavior is known as hyperelasticity, and the material which shows this behavior is called green elastic material or hyperelastic. A hyperelastic material differs from an elastic material in four main aspects:

- The tire has a high stiffness in the initial step of loading, and dramatically softens in the unloading phase. This phenomenon is known as Mullin's effect.
- Instead of having a hysteresis loop in the stress-strain curves of the loading cycle, the hyperelastic materials have a simple equilibrium curve.
- The hyperelastic materials exhibit different behavior in tension and compression. This is in contrast with the Hooke's law, which considers the stress to be proportional to strain. As a matter of fact, hyperelastic materials such as rubber, have a higher stress magnitude in compression when compared to the tension for an identical strain magnitude.

- Finally, a hyperelastic material has different modes of deformation that should be studied with respect to the given loading conditions. Each deformation mode requires corresponding constants in the material model that must be characterized experimentally. The choice of model constants and required parameterization tests should be done with care in order to avoid false analytical system response quantities that are not present in the experiments.

The hyperelasticity feature of the rubber should be enhanced with the viscoelasticity in order to precisely describe the rate-dependent loading/unloading force-deflection characteristics of the tire.

3.2 Viscoelasticity

Viscoelastic materials show a combined elastic and viscous rate-dependent behavior when experiencing deformation [29]. In elastic materials, once the applied stress or strain is removed, the specimen quickly returns to its initial condition. On the other hand, viscous materials exhibit a resistance toward the shear flow developed due to the applied stress or strain. In other words, upon applying a constant strain, the material creeps. Similarly, by applying a constant stress, the strain increases and then eventually decreases with time.

The internal damping, rolling resistance, and thermal characteristics of a tire are associated with the viscoelastic property of the rubber. Therefore, in order to properly quantify the transient response of the tire, the viscoelastic material property should be incorporated. For small strains, the linear viscoelasticity assumption may be chosen. In this case, the relaxation rate of the material is proportional to the immediate stress, and the total viscoelastic behavior can be expressed using the superposition principle.

3.3 Modeling procedure

There are different mechanical models that can describe the combined hyperelastic viscoelastic characteristics of a material. Each of the mechanical models considers a certain form of stress or strain response for the material under different loading conditions. The hyperelasticity of the tire is modeled by interpolating the tire load vs. deflection data in compression/tension loading/unloading scenarios. Using this approach allows us to define different loading stiffness for loading and unloading paths.

To include viscoelasticity, three main models considered which are Maxwell model, Kelvin-Voigt model, and Standard Linear Solid model [30]. For the Maxwell model, the viscoelasticity is modeled using a damping element

(Newtonian dashpot) connected to a Hookean spring (stiffness element) in a series configuration. Considering the fact that the Maxwell model exhibits the unrestricted flow of material during loading, it isn't desirable for the rubber element modeling. For the Kelvin-Voigt element, the stiffness and the damping elements are connected to each other in a parallel configuration. The force-deflection characteristics of this model for force step input and deflection step input are shown in Figure 2.

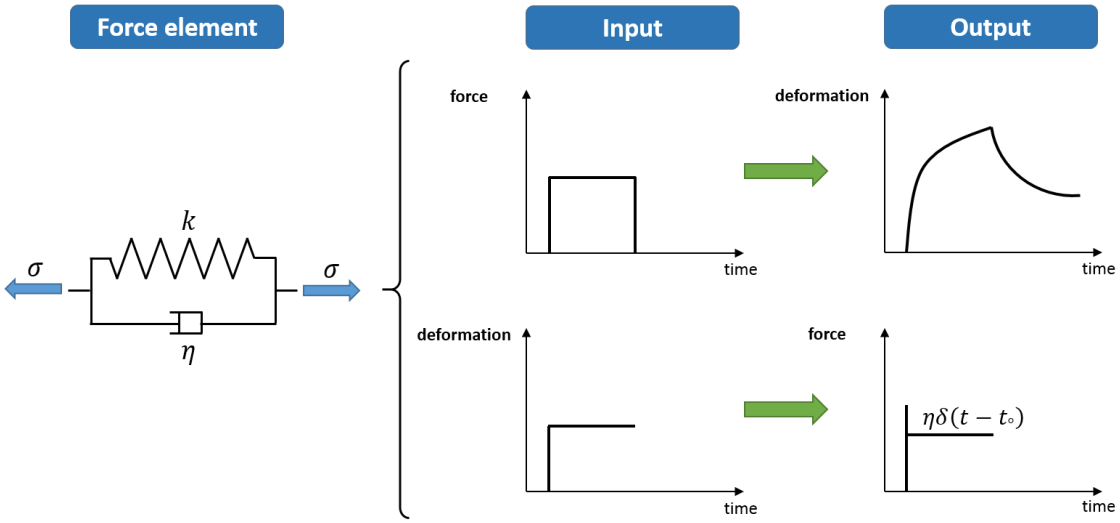

Figure. 2 - The force-deflection characteristics of the Kevin-Voigt model for force step input and deflection step input.

For this type of element, the force-deflection relation under axial loading has the following form:

$$\sigma = k\varepsilon + \eta \frac{d\varepsilon}{dt} \tag{1}$$

Where k is the axial stiffness, η is the damping stiffness, ε is the element strain, and σ is the applied stress. It should be noted that stress and strain of the element are analogous to the force and deflection. In the multi-axial loading the equation of motion is written as

$$S_{ij} = Ke_{ij} + \eta \frac{de_{ij}}{dt} \tag{2}$$

In which K is the time-dependent bulk modulus, and S_{ij} is the element compliance. Another material model of interest is the Standard Linear Model (SLM), which is a Maxwell model that is connected to another stiffness element in a parallel configuration. It is cumbersome to solve for the stress value in the Maxwell arm, since it contains both the

stress and its derivative. Therefore, the Kevin-Voigt element is used as the main force element between tire/rim elements due to the fact that it is more accurate compare to the Maxwell model, and easier to solve for the stress values compare to the SLM.

4 Tire structure modeling

As it was discussed earlier, the detailed modeling of the tire structure is not required for studying the mobility of the tire. This is due to the fact that, for evaluating the tire performance, only a limited number of parameters are needed, such as forces and moments at the spindle, and wheel sinkage. Therefore, modeling the tire with a coarse level of tire structure discretization would be adequate, and can result in a fast computational time. This feature is essential for full vehicle simulations and control applications. The lumped parameter models reduce the DOFs in the model in favor of the computational effort, and consider the simplified material models in the respective directions. Such a method is used in HSSTM for representing the tire structure.

In the early phase of the project, a simplified lumped mass approach for modeling the tire structure was introduced by Pinto [31-33]. This approach considered the tire structure as three layers of lumped masses, in which the masses are connected to the rim and also to each other through a set of linear spring and dampers. This three-layer structure approach is an advanced version of a lumped mass single layer on-road tire model developed by Umsrithong [34-39]. In 2012, an advanced method for modeling the tire was introduced [29], and a more systematic approach was used for developing the software. In this new approach, the tire belt is discretized circumferentially in multiple belt segments that are suspended on the rim using Kelvin-Voigt elements, which include variable stiffness and damping. These nonlinear elements capture the effect of the temperature and pressure changes on the tire mechanical characteristics through a set of empirical equations. Each belt segment is divided into a series of lumped masses connected to each other with in-plane and out-of-plane spring and dampers. The dynamics of these lumped masses, in addition to wheel, is described in a state-space representation. The state is a set of variables that, along with the time step, characterize the individual configuration of the system at any instance of time. The state variables are defined by equations of motion, and can be positions, velocities, acceleration, force, moment, torque, pressure, and etc. The state variables that are described using the differential equations are called state differential variables, and those that are defined directly from dynamic conditions, are called extra state variables. The standard notational convention for describing

a state-space representation is as follows:

State equation: $\dot{q}(t)_{[N\times1]} = A(t)_{[N\times N]}q(t)_{[N\times1]} + B(t)_{[N\times M]}u(t)_{[M\times1]}$ (3)

Output equation: $v(t)_{[P\times1]} = C(t)_{[P\times N]}q(t)_{[N\times1]} + D(t)_{[P\times M]}u(t)_{[M\times1]}$ (4)

Where $q(t)$ is the state vector, $\dot{q}(t)$ is the derivative of the state vector, $A(t)$ is the state matrix, $B(t)$ is the input matrix, $C(t)$ is the output matrix, $D(t)$ is the direct transmission matrix, $u(t)$ is the input vector, $v(t)$ is the output vector, N is the number of states, M is the number of input variables, and P is the number of output variables. It should be noted that the input, output, and state vectors, as well as all the state-space representation matrices are time dependent. The choice of the state variables for different sections of the tire model is not unique, and would be discussed accordingly in the following sections. The type of mathematical model used to represent the tire structure is called a tire realization.

After discretizing the tire into smaller elements, we can express the dynamics of each element using a set of first order and second order differential equations. The second order differential equations can be rearranged as a set of first order ODEs. The complete set of the ODEs can be shown as follows:

$$\left\{\begin{array}{l}\dot{q}_1 = f_1(x_1,...,x_N,u_1,...,u_M,t)\\ \vdots\\ \dot{q}_N = f_N(x_1,...,x_N,u_1,...,u_M,t)\end{array}\right\} \quad (5)$$

$$\left\{\begin{array}{l}\dot{v}_1 = g_1(x_1,...,x_N,u_1,...,u_M,t)\\ \vdots\\ \dot{v}_N = g_N(x_1,...,x_N,u_1,...,u_M,t)\end{array}\right\} \quad (6)$$

Where $f_i(i=1,...,N)$, and $f_j(j=1,...,N)g_j$ $(j = 1 \ldots P)$ include the following: (1) nonlinear functions of states and/or inputs, such as *Sin* and *Cos* functions, (2) terms with states and/or inputs appearing as powers of something other than 1 and 0, (3) terms with cross products of states and/or inputs. As a results, the multi-segments model that represent the tire characteristics is an autonomous (time-variant) non-linear system.

4.1 Coordinate system convention

Before defining the state variables of the system, the coordinate systems for the sign convention must be defined. The definitions for the coordinate systems used in this study are similar to the Tyre Data Exchange format (TYDEX). TYDEX is a conventional interface between tire measurements and tire models developed and unified by an international tire working group to make the tire measurement data exchange easier. Additionally, TYDEX introduce an interface between the tire model and simulation tool called Standard Tire Interface (STI), which would be described in detail later on.

Along with the global reference frame, one additional right-hand orthogonal axis system used is the C-axis system (center axis system), as shown in Figure 3. The angles of rotation illustrated in this figure are: a positive slip angle α, a positive inclination angle γ, and a positive wheel rotation speed ω. The C-axis coordinate origin is mounted at the center of the wheel rim. The X_c axis is in the central wheel plane and is parallel to the ground. The central wheel plane is constructed by decreasing the width of the wheel until it becomes a rigid disk with zero width. The Y_c axis is same as the spin axis of the wheel and rotates with the inclination angle γ. The Z_c axis is in the central plane of the wheel, point upwards, and turns with the inclination angle γ (camber).

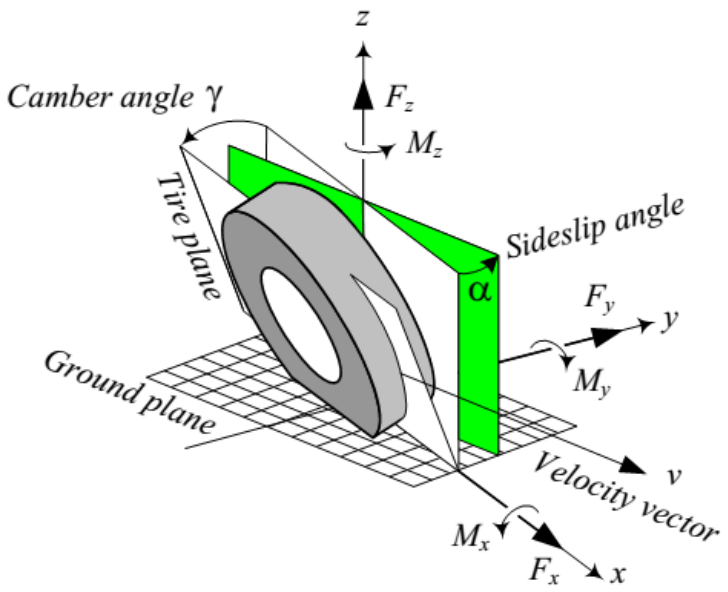

Figure. 3 - The representation of the C-axis coordinate system.

4.2 Wheel system

The rim kinematics can be described using six degrees of freedom (DOF) resulting in 12 state variables. Consider

the position state vector of the wheel system as following:

$$ {}^{pos}_{rim}q = \begin{bmatrix} x_{rim} \\ y_{rim} \\ z_{rim} \\ \alpha_{rim} \\ \beta_{rim} \\ \delta_{rim} \end{bmatrix} \tag{7} $$

Where x_{rim}, y_{rim}, and z_{rim} are the translational coordinates of the wheel center in the global reference frame, α_{rim} is the wheel rotation angel around global *X* axis, β_{rim} is the wheel rotation angel around global *Y* axis, and δ_{rim} is the wheel rotation angel around *Z* axis. Furthermore, the velocity state vector of the wheel system is

$$ {}^{vel}_{rim}q = \begin{bmatrix} \dot{x}_{rim} \\ \dot{y}_{rim} \\ \dot{z}_{rim} \\ \omega_x \\ \omega_y \\ \omega_z \end{bmatrix} \tag{8} $$

Where $\dot{x}_{rim}$, $\dot{y}_{rim}$, and $\dot{z}_{rim}$ are rim center translational velocities along global *X*, *Y*, and *Z* axes described in the global reference frame. Also ω_x, ω_y, and ω_z are rim center rotational velocities around global *X*, *Y*, and *Z* axes described in the global reference frame. Therefore, the final state vector of the wheel is given as:

$$ {}_{rim}q = \begin{bmatrix} {}^{pos}_{rim}q \\ {}^{vel}_{rim}q \end{bmatrix} \tag{9} $$

4.3 Tire belt

If we discretize the tire belt circumference into N_{belt_seg} segments, the angle between the centers of each two segment will be

$$\Delta\theta_{seg} = \frac{2\pi}{N_{belt\_seg}} \tag{10}$$

Next, each segment is divided into N_{seg_elm} segment elements. The number of belt elements is assumed to be an odd number greater than three in order to always have at least one node at the middle of tire width and two neighboring nodes. Each segment element is actually a lumped mass with only translational DOF. Eliminating the rotational DOF from the belt segments helps reduce the computational effort of the model, while maintaining its accuracy. Consequently, the state vector for the segment elements is written as:

$$_{seg}q = \begin{bmatrix} {}^{pos}_{seg}q_i \\ {}^{vel}_{seg}q_i \end{bmatrix} \qquad i = 1,\ldots,N_{belt\_seg} \tag{11}$$

Where

$${}^{pos}_{seg}q_i = \begin{bmatrix} x_j \\ y_j \\ z_j \end{bmatrix}_i \qquad j = 1,\ldots,N_{seg\_elm} \tag{12}$$

$${}^{vel}_{seg}q_i = \begin{bmatrix} x_j \\ y_j \\ z_j \end{bmatrix}_i \qquad j = 1,\ldots,N_{seg\_elm} \tag{13}$$

4.4 Pressure effect

The general behavior of the tire depends substantially on tire inflation pressure. As the tire is loaded, its stiffness increases non-linearly. Meanwhile, there is a constant term in load-deflection curves of the tire mass elements due to the inner pressure force. The air pressure results in a directional force on each of the mass points. This force is calculated using the following formula:

$$F_{pressure} = \frac{\pi \cdot r_{belt}}{n_{segments}} \cdot width_{tread} \cdot P_{actual} \tag{14}$$

Furthermore, to include the pressure change effects on the tire structure, the tire stiffness in the radial direction is updated at each time step based on the tire inflation pressure:

$$K_{\mathrm{mod}ified} = \left(a_1 + a_2 \cdot \frac{p_{actual}}{p_{measured}} \right) \cdot K_{measured} \tag{15}$$

Where a_1 and a_2 are constant terms, which are specified based on curve fitting developed finite element tire model simulation results at different tire pressures. This procedure results in a look-up table, which is used for interpolating the relative stiffness of the tire in radial direction and at every normal load.

4.5 Tire tread

In order to incorporate the tread design, a certain number of brush elements are assigned to each belt element in a rectangular array. Consider an array of bristles with N_{tread_circ} elements in the circumferential direction and N_{tread_lat} elements in the lateral direction. As a result, the number of total sensor points assigned to each belt element will be:

$$N_{tread\_total} = N_{tread\_circ} \times N_{tread\_lat} \tag{16}$$

Each brush element is a massless bristle that has translational stiffness in radial, longitudinal, and lateral directions. The base of these bristles is connected to each lumped mass (element segment), and the tip is touching the ground. This massless tip acts as a sensor point and can be used to detect the tire-road contact. Also, using the direction and value of the deflection in the bristle, the ground forces generated are calculated. Through implementation of the sensor points, we are able to increase the resolution of the contact patch by having more contact detection points at this area. At the same time, to define their velocities in space, these massless points only require extrapolation of the position and velocity of the nearby belt elements without the need for differential equations. Based on the findings of [5],there are only three state variables needed to describe the position of the brush tips in the space. These variables store the displacements of the brush tips in the global reference frame from previous iterations of the solver. Therefore, the state vector of each brush element will be:

$$_{brush}q_{i,j}^{m,n} = \begin{bmatrix} \lambda_{i,j}^{(1)} \\ \lambda_{i,j}^{(2)} \\ \lambda_{i,j}^{(3)} \end{bmatrix} \qquad \begin{cases} i = 1,\ldots, N_{tread\_lat} \\ j = 1,\ldots, N_{tread\_circ} \end{cases} \tag{17}$$

Where *m* and *n* are the indices for the associated n^{th} belt element in the m^{th} belt segment. The final state vector of the system can be constructed as follows:

$$ {}_{total}q = \begin{bmatrix} {}_{rim}q \\ {}_{seg}q \\ {}_{brush}q \end{bmatrix} \tag{18} $$

4.6 Initial position initialization

The initial position of the rim is expressed in the global reference frame by:

$$ {}^{G}_{rim}r_{o} = \begin{bmatrix} x_{\circ} \\ y_{\circ} \\ z_{\circ} \end{bmatrix} \tag{19} $$

The initial position of the tire elements depends on the tire geometrical properties, as well as the rim initial camber and slip angles. Consider the tire element P, with the position vector ${}^{W}r$ described in the wheel local reference frame noted as C-Axis. If this reference frame rotates around global *X*, *Y*, and *Z* axes with ψ, θ, and ϕ respectively, the coordinates of the point P in the global and in the rim local reference frames can be related using the equation:

$$ {}^{G}r = R_{total}\,{}^{W}r \tag{20} $$

Where R_{total} is the total transformation matrix after three consecutive rotations and can be calculated by multiplying individual transformation matrices for the rotation around each axis respectively:

$$ R_{total} = R_{Y,\theta}R_{X,\psi}R_{Z,\phi} \tag{21} $$

$$ R_{Y,\theta} = \begin{bmatrix} \cos(\theta) & 0 & \sin(\theta) \\ 0 & 1 & 0 \\ -\sin(\theta) & 0 & \cos(\theta) \end{bmatrix} \tag{22} $$

$$ R_{Z,\phi} = \begin{bmatrix} \cos(\phi) & -\sin(\phi) & 0 \\ \sin(\phi) & \cos(\phi) & 0 \\ 0 & 0 & 1 \end{bmatrix} \tag{23} $$

$$R_{X,\psi} = \begin{bmatrix} 1 & 0 & 0 \\ 0 & \cos(\psi) & -\sin(\psi) \\ 0 & \sin(\psi) & \cos(\psi) \end{bmatrix} \tag{24}$$

The position vector of the j^{th} element in the first tire segment is:

$${}^{W}_{seg}r_{1,j} = \begin{bmatrix} tire\_radius \\ \left(j - \dfrac{N_{seg\_elm}+1}{2} \right) \times \Delta y_{seg\_elm} \\ 0 \end{bmatrix} \tag{25}$$

Where Δy_{seg_elm} is the lateral displacement between the centers of two adjacent elements in each tire segment:

$$\Delta y_{seg\_elm} = \frac{tire\_width}{N_{seg\_elm} - 1} \tag{26}$$

Consequently the local position of the j^{th} element in the i^{th} segment is:

$${}^{W}_{seg}r_{i,j} = R_{Y,(\Delta\theta_{seg} \times i)} \times {}^{W}_{seg}r_{1,j} \tag{27}$$

Where $\Delta\theta_{seg}$ is the angular difference between two adjacent belt segments:

$$\Delta\theta_{seg} = \frac{2\pi}{N_{belt\_seg}} \tag{28}$$

The initial position of the j^{th} element in the i^{th} belt segment described in the global reference frame can be expressed as:

$${}^{G}_{seg}r_{i,j} = {}^{G}_{rim}r_{o} + R_{Z,(Slip\_angle)} \times R_{Z,(Camber\_angle)} \times {}^{W}_{seg}r_{i,j} \tag{29}$$

Finally, the initial state vector of the system becomes:

$${}_{total}q_{\circ} = \begin{bmatrix} {}_{rim}q_{\circ} \\ {}_{seg}q_{\circ} \\ {}_{brush}q_{\circ} \end{bmatrix} \tag{30}$$

4.7 Tire model kinematics

In order to write the equations of motion for the rim and the lumped masses, the internal forces between the tire elements and the rim should be identified. The Kevin-Voigt force elements that connect tire belt elements to each other and to the rim generate the internal forces as functions of relative displacement and relative velocity of lumped masses with respect to the rim circumference. Therefore, formulating the model kinematics is essential for calculating the kinetics of the elements. In this section, a set of kinematic parameters that are required for writing the model equations of motion are introduced.

The transformation matrix for the i^{th} belt segment is defined as:

$$R_{tot}^{i} = R_{Z,\phi_{rim}} \times R_{X,\psi_{rim}} \times R_{Y,\left(\theta_{rim}+\Delta\theta_{seg}\times i\right)} \tag{31}$$

For the un-inflated tire, the unity vector ${}^{G}_{cw}r_{i}$ normal to the center of the i^{th} belt segment, which passes through the rim center is given as:

$${}^{G}_{cw}r_{i} = R_{tot}^{i} \times \begin{bmatrix} Tire\_radius \\ 0 \\ 0 \end{bmatrix} \tag{32}$$

$${}^{G\ \wedge}_{cw}r_{i} = \frac{{}^{G}_{cw}r_{i}}{\left|{}^{G}_{cw}r_{i}\right|} \tag{33}$$

The vector from the rim center to the j^{th} element of the i^{th} belt segment of the tire is:

$${}^{G}_{cwo}r_{i,j} = R_{tot}^{i} \times \begin{bmatrix} Tire\_radius \\ \left(j - \dfrac{N_{seg\_elm}+1}{2}\right)\Delta y_{seg\_elm} \\ 0 \end{bmatrix} \tag{34}$$

$${}^{G\ \wedge}_{cwo}r_{i,j} = \frac{{}^{G}_{cwo}r_{i,j}}{\left|{}^{G}_{cwo}r_{i,j}\right|} \tag{35}$$

The relative position of the first belt element near the left sidewall in the i^{th} belt segment from its projection on the rim is given as:

$$ {}^{G}_{wtl}r_i = {}^{G}_{tire}r_{i,N_{belt\_seg}} - {}^{G}_{rim}r_{i,N_{belt\_seg}} \tag{36} $$

Similarly, the relative position of the last belt element near the right sidewall in the i^{th} belt segment from its projection on the rim is given as:

$$ {}^{G}_{wtr}r_i = {}^{G}_{tire}r_{i,1} - {}^{G}_{rim}r_{i,1} \tag{37} $$

For the intermediate belt elements located between the first and last elements, which are directly connected to the rim, the relative position of each element from the center of its left and right neighbor elements are:

$$ {}_{left\_elm}{}^{G}r_{i,j} = {}^{G}_{tire}r_{i,j} - {}^{G}_{tire}r_{i,j+1} \qquad j = 2,..., N_{seg\_elm} - 1 \tag{38} $$

$$ {}_{right\_elm}{}^{G}r_{i,j} = {}^{G}_{tire}r_{i,j} - {}^{G}_{tire}r_{i,j-1} \qquad j = 2,..., N_{seg\_elm} - 1 \tag{39} $$

The relative position of the tread block center from its neighbor j^{th} belt element is:

$$ {}^{G}_{tread}r_{i,j} = {}^{G}_{tire}r_{i,j} + \left|tread\_tickness\right| \times_{cw} \hat{r}_i \tag{40} $$

The local coordinate system at the center of the i^{th} belt segment described in global reference frame is:

$$ {}^{G}_{tread}r_{i,j} = {}^{G}_{tire}r_{i,j} + \left|tread\_tickness\right| \times_{cw} \hat{r}_i \tag{41} $$

The position of the point P described at the local reference frame of the i^{th} belt segment is:

$$ {}_{belt}P^i = p_1 \cdot e_1^i + p_2 \cdot e_2^i + p_3 \cdot e_3^i \tag{42} $$

Where

$$ e_1^i = \frac{\tilde{e}_2^i \times_{cw} \hat{r}_i}{\left\| \tilde{e}_2^i \times_{cw} \hat{r}_i \right\|}, \quad e_2^i = \frac{R_{Z,\phi_{rim}} \times R_{X,\psi_{rim}} \times \begin{bmatrix} 0 & 1 & 0 \end{bmatrix}^T}{\left\| R_{Z,\phi_{rim}} \times R_{X,\psi_{rim}} \times \begin{bmatrix} 0 & 1 & 0 \end{bmatrix}^T \right\|}, \quad e_3^i = {}_{cw}\hat{r}_i \tag{43} $$

$$\tilde{e}_2^i = \begin{bmatrix} 0 & -e_{2z}^1 & e_{2y}^i \\ e_{2z}^i & 0 & -e_{2x}^i \\ -e_{2y}^i & e_{2x}^i & 0 \end{bmatrix} \tag{44}$$

The tire structural stiffness and damping behaviors are simulated using the tire model Voigt elements. The force that is produced by a Voigt element is proportional to its length and the relative velocity between its two ends. The direction of this force is parallel to the element centerline. Therefore, the position and velocity of the force element tips relative to their bases should be calculated.

The relative distance between a lumped mass in the j^{th} belt element and its projected position on the rim, described in the i^{th} belt segment local reference frame is expressed as:

$${}_{belt}D^{i,j} = DT_1^{i,j} \cdot e_1^i + DT_2^{i,j} \cdot e_2^i + DT_3^{i,j} \cdot e_3^i \tag{45}$$

Where

$$\begin{bmatrix} DT_1 \\ DT_2 \\ DT_3 \end{bmatrix}^{i,N_{belt\_elm}} = \begin{bmatrix} e_1^i \\ e_2^i \\ e_3^i \end{bmatrix}^T \cdot {}_{wtl}^{G}r \tag{46}$$

$$\begin{bmatrix} DT_1 \\ DT_2 \\ DT_3 \end{bmatrix}^{i,1} = \begin{bmatrix} e_1^i \\ e_2^i \\ e_3^i \end{bmatrix}^T \cdot {}_{wtr}^{G}r \tag{47}$$

The relative distance between the center of the j^{th} belt element and its left and right belt element neighbors, described in the i^{th} belt segment local reference frame is given as:

$$\begin{bmatrix} DBL_1 \\ DBL_2 \\ DBL_3 \end{bmatrix}^{i,j} = \begin{bmatrix} e_1^i \\ e_2^i \\ e_3^i \end{bmatrix}^T \cdot {}_{left\_elm}^{G}r_{i,j} \qquad j = 1,\ldots,N_{seg\_elm} - 1 \tag{48}$$

$$\begin{bmatrix} DBR_1 \\ DBR_2 \\ DBR_3 \end{bmatrix}^{i,j} = \begin{bmatrix} e_1^i \\ e_2^i \\ e_3^i \end{bmatrix}^T \cdot {}^{G}_{wtl}r - {}^{G}_{right\_elm}r_{i,j} \qquad j = 2,...,N_{seg\_elm} \tag{49}$$

Relative velocity measurements

$${}^{W}DT\,D = \dot{DT}_1^{i,j} \times e_1^i + \dot{DT}_2^{i,j} \times e_2^i + \dot{DT}_3^{i,j} \times e_3^i \tag{50}$$

$$\begin{bmatrix} \dot{DT}_1 \\ \dot{DT}_2 \\ \dot{DT}_3 \end{bmatrix}^{i,N_{belt\_elm}} = \begin{bmatrix} e_1^i \\ e_2^i \\ e_3^i \end{bmatrix}^T \cdot {}^{G}_{wtl}\dot{r}^i \tag{51}$$

$$\begin{bmatrix} \dot{DT}_1 \\ \dot{DT}_2 \\ \dot{DT}_3 \end{bmatrix}^{i,1} = \begin{bmatrix} e_1^i \\ e_2^i \\ e_3^i \end{bmatrix}^T \cdot {}^{G}_{wtr}\dot{r}^i \tag{52}$$

$$\begin{bmatrix} \dot{DBL}_1 \\ \dot{DBL}_2 \\ \dot{DBL}_3 \end{bmatrix}^{i,j} = \begin{bmatrix} e_1^i \\ e_2^i \\ e_3^i \end{bmatrix}^T \cdot {}^{G}_{left\_elm}\dot{r}_{i,j} \qquad j = 1,...,N_{seg\_elm} - 1 \tag{53}$$

$$\begin{bmatrix} \dot{DBR}_1 \\ \dot{DBR}_2 \\ \dot{DBR}_3 \end{bmatrix}^{i,j} = \begin{bmatrix} e_1^i \\ e_2^i \\ e_3^i \end{bmatrix}^T \cdot {}^{G}_{right\_elm}\dot{r}_{i,j} \qquad j = 2,...,N_{seg\_elm} \tag{54}$$

Where

$${}^{G}_{left\_elm}\dot{r}_{i,j} = {}^{G}_{tire}\dot{r}_{i,j} - {}^{G}_{tire}\dot{r}_{i,j+1} \tag{55}$$

$$ {}^{G}_{right\_elm}\dot{r}_{i,j} = {}^{G}_{tire}\dot{r}_{i,j} - {}^{G}_{tire}\dot{r}_{i,j-1} \tag{56} $$

Velocity of a point located at the projection of the j^{th} belt element in the i^{th} belt segment on the rim circumference, and described in the i^{th} belt segment local reference frame is:

$$ {}^{W}_{rim\_circ}v_{i,j} = \begin{bmatrix} e_1^i \\ e_2^i \\ e_3^i \end{bmatrix}^T \cdot {}_{rim\_circ}{}^{G}v_{i,j} \tag{57} $$

$$ {}^{G}_{rim\_circ}v_{i,j} = v_{rim} + \tilde{\Omega}_{rim} \times {}_{cwo}\hat{r}_{i,j} \tag{58} $$

4.8 Tire model kinematics

The components of the left sidewall force vector between i^{th} belt segment and the rim are calculated as:

$$ \begin{bmatrix} FL_1 \\ FL_2 \\ Fl_3 \end{bmatrix}^i = \begin{bmatrix} e_1^i \\ e_2^i \\ e_3^i \end{bmatrix}^T \cdot \begin{bmatrix} -k_{t1} \cdot \left(DT_1^{i,N_{belt\_elm}}\right) - c_{t1}\left(\dot{DT}_1^{i,N_{belt\_elm}} - \left({}^{W}_{rim\_circ}v_{i,N_{belt\_elm}}\right)_1\right) \\ -k_{t2} \cdot \left(DT_2^{i,N_{belt\_elm}}\right) - c_{t2}\left(\dot{DT}_2^{i,N_{belt\_elm}} - \left({}^{W}_{rim\_circ}v_{i,N_{belt\_elm}}\right)_2\right) \\ -k_n \cdot \left(DT_3^{i,N_{belt\_elm}} - h_{carcass}\right) - c_n\left(\dot{DT}_3^{i,N_{belt\_elm}} - \left({}^{W}_{rim\_circ}v_{i,N_{belt\_elm}}\right)_3\right) \end{bmatrix} \tag{59} $$

Where $h_{carcass}$ is the tire carcass height, k_{t1} is tire sidewall tangential stiffness, c_{t1} is tire sidewall tangential damping, k_{t2} is tire sidewall lateral stiffness, c_{t2} is tire sidewall lateral damping, k_n is tire sidewall radial stiffness, and c_n is tire sidewall radial damping. The resultant force that is applied to the i^{th} belt segment by the rim from the left sidewall is given as

$$ {}^{W}_{sidewall}FL^{i,j} = FL_1^i + FL_2^i + FL_3^i \tag{60} $$

Similarly for the force vector in the right sidewall between tire and the rim we have:

$$\begin{bmatrix} FR_1 \\ FR_2 \\ FR_3 \end{bmatrix}^i = \begin{bmatrix} e_1^i \\ e_2^i \\ e_3^i \end{bmatrix}^T \cdot \begin{bmatrix} -k_{t1} \cdot \left(DT_1^{i,1}\right) - c_{t1}\left(\dot{DT}_1^{i,1} - \left({}^{W}_{rim\_circ}v_{i,1} \right)_1 \right) \\ -k_{t2} \cdot \left(DT_2^{i,1}\right) - c_{t2}\left(\dot{DT}_2^{i,1} - \left({}^{W}_{rim\_circ}v_{i,1} \right)_2 \right) \\ -k_{n} \cdot \left(DT_3^{i,1} - h_{carcass}\right) - c_{n}\left(\dot{DT}_3^{i,1} - \left({}^{W}_{rim\_circ}v_{i,1} \right)_3 \right) \end{bmatrix} \tag{61}$$

The resultant force that is applied to the i^{th} belt segment by the rim from the right the sidewall is given as:

$${}^{W}_{sidewall}FR^{i,j} = FR_1^i + FR_2^i + FR_3^i \tag{62}$$

Next, the force components within the belt segment that are generated between the neighboring belt elements are calculated. The forces exerted to the j^{th} belt element in the i^{th} belt segment by its neighboring elements are:

$$\begin{bmatrix} FB_1 \\ FB_2 \\ FB_3 \end{bmatrix}^{i,j} = \left(e^i\right)^T \cdot \left[K_{belt} \cdot \left(DBR^{i,j} + DBL^{i,j}\right) - C_{belt} \cdot \left(\dot{DBR}^{i,j} + \dot{DBL}^{i,j} - {}^{G}_{rightt\_elm}\dot{r}_{i,j} - {}^{G}_{left\_elm}\dot{r}_{i,j} \right) \right] \tag{63}$$

Where K_{belt} is the tire belt stiffness matrix and is defined as:

$$K_{belt} = \begin{bmatrix} k_{bt1} & 0 & 0 \\ 0 & k_{bt2} & 0 \\ 0 & 0 & k_n \end{bmatrix} \tag{64}$$

In the tire belt mass matrix, k_{bt1} is the tire belt inner-tangential stiffness, k_{bt2} is the tire belt inner-lateral stiffness, and k_{bn} is the tire belt inner-radial stiffness. Moreover, C_{belt} is the tire belt damping matrix, which is defined as:

$$C_{belt} = \begin{bmatrix} c_{bt1} & 0 & 0 \\ 0 & c_{bt2} & 0 \\ 0 & 0 & c_n \end{bmatrix} \tag{65}$$

In the tire belt damping matrix, c_{bt1} is tire belt inner-tangential damping, c_{bt2} is tire belt inner-lateral damping, and c_{bn} is tire belt inner-radial damping. The total force vector that exerted to the j^{th} belt element in the i^{th} belt segment from its neighbor elements can be identified as:

$$ {}^{W}FB^{i,j} = FB_1^{i,j} + FB_2^{i,j} + FB_3^{i,j} \tag{66} $$

Therefore, the total structural forces on the j^{th} belt element in the i^{th} belt segment is given as:

$$ {}^{W}_{structure}F^{i,j} = {}^{W}FB^{i,j} + {}^{W}_{sidewall}FL^{i,j} + {}^{W}_{sidewall}FR^{i,j} \tag{67} $$

Finally, the total internal force that is applied to the belt element can be written as:

$$ {}^{W}_{internal}F^{i,j} = {}^{W}_{structure}F^{i,j} + \begin{bmatrix} 0 \\ 0 \\ -mg \end{bmatrix} + F^{i,j}\left(r_{tire}, t\right) \cdot \hat{e}_3 \tag{68} $$

The torque from the tire i^{th} belt segment to the rim is written as:

$$ {}^{W}_{belt}T^{i} = {}_{cwo}\tilde{r}^{i,1} \times {}^{W}_{structure}F^{i,1} + {}_{cwo}\tilde{r}^{i,N_{belt\_elm}} \times {}^{W}_{structure}F^{i,N_{belt\_elm}} \tag{69} $$

Where

$$ \tilde{e}_2^i = \begin{bmatrix} 0 & -{}_{cwo}\tilde{r}_3^{i,j} & -{}_{cwo}\tilde{r}_2^{i,j} \\ -{}_{cwo}\tilde{r}_3^{i,j} & 0 & -{}_{cwo}\tilde{r}_1^{i,j} \\ -{}_{cwo}\tilde{r}_2^{i,j} & -{}_{cwo}\tilde{r}_1^{i,j} & 0 \end{bmatrix} \tag{70} $$

After calculating the individual force components applied to each lumped mass, we can write the equation of motion such as:

$$ \begin{bmatrix} \ddot{x} \\ \ddot{y} \\ \ddot{z} \end{bmatrix} = \frac{1}{m}\left\{ {}_{structural}F + {}_{internal}F + {}_{external}F + {}_{gravity}F \right\} \tag{71} $$

$$ {}_{lumped\_mass}{}^{G}q^{i,j} = \begin{bmatrix} x & \dot{x} & y & \dot{y} & z & \dot{z} \end{bmatrix} \tag{72} $$

For simplicity, the rim is considered as a spatial rigid body. As a result, three translational and three rotational DOF are used for describing its motion:

$$m \cdot \ddot{r} = {}^{G}F = {}^{G}_{rim}F + \sum_{belt} F^{i} \tag{73}$$

$$J \cdot \ddot{\phi} = {}^{G}M = {}_{rim}M + \sum_{bet} M^{i} \tag{74}$$

Where ${}_{rim}F$ is the applied force vector to the rim center, ${}_{belt}F^{i}$ is the structural force from the i^{th} belt segment, ${}_{rim}M$ is the applied torque vector to the rim center, and ${}_{belt}M^{i}$ is the applied toque vector from i^{th} belt segment to the rim center, and is given as:

$$\sum_{bet} M^{i} = \sum \left[\left({}_{rim\_circ}r - {}_{rim}r \right) \times F^{i} \right] \tag{75}$$

The rim translational dynamics is represented in the global reference frame as follows:

$${}^{G}F = m \cdot \left({}^{G}_{rim}a \right) = m \cdot \left({}^{G}_{rim}\ddot{r} \right) \tag{76}$$

Consequently, rim translational equations of motion expressed in the rim local reference frame are given as:

$${}^{W}F = {}^{W}R_{G}\,{}^{G}F = m\,{}^{W}R_{G}\,{}^{G}_{rim}\ddot{r} = m\left({}^{B}_{rim}\ddot{r} \right) + m\left({}^{W}\omega \times {}^{W}_{rim}\dot{r} \right) \tag{77}$$

With the following vector form:

$${}^{W}\begin{bmatrix} F_x \\ F_y \\ F_z \end{bmatrix} = m\,{}^{W}\begin{bmatrix} \ddot{r}_x \\ \ddot{r}_y \\ \ddot{r}_z \end{bmatrix} + m\,{}^{W}\begin{bmatrix} w_x \\ w_y \\ w_z \end{bmatrix} \times {}^{W}\begin{bmatrix} \dot{r}_x \\ \dot{r}_y \\ \dot{r}_z \end{bmatrix} = m\,{}^{W}\begin{bmatrix} \ddot{r}_x + \left(w_y \dot{r}_z - w_z \dot{r}_y \right) \\ \ddot{r}_y + \left(w_x \dot{r}_z - w_z \dot{r}_x \right) \\ \ddot{r}_z + \left(w_x \dot{r}_y - w_y \dot{r}_x \right) \end{bmatrix} \tag{78}$$

The applied forces to the rim center consist of the axle forces and suspension forces:

$${}^{G}_{rim}F = {}^{G}_{axle}F + {}^{G}_{suspension}F \tag{79}$$

Next, the rotational dynamics for the rim is studied. The applied moment to the rim from the axle, described in the rim local reference frame, is given as:

$$ {}^{W}_{rim}M = M_x \hat{i} + M_y \hat{j} + M_z \hat{k} = I_{rim} {}^{W}\dot{\omega} + {}^{W}_{rim}\omega \times \left(I_{rim} {}^{W}\omega \right) \tag{80} $$

Where ${}^{W}_{rim}\omega$ is the rim angular velocity vector, and I is the inertia matrix, which is written as:

$$ I = \begin{bmatrix} I_{xx} & I_{xy} & I_{xz} \\ I_{yx} & I_{yy} & I_{yz} \\ I_{zx} & I_{zy} & I_{zz} \end{bmatrix} \tag{81} $$

Additionally, the components of the torque vector are described as:

$$ M_x = I_{xx}\dot{\omega}_x + I_{xy}\dot{\omega}_y + I_{xz}\dot{\omega}_z - \left(I_{yy} - I_{zz}\right)\omega_y\omega_z - I_{yz}\left(\omega_z^2 - \omega_y^2\right) - \omega_x\left(\omega_z I_{xy} - \omega_y I_{xz}\right) \tag{82} $$

$$ M_y = I_{yx}\dot{\omega}_x + I_{yy}\dot{\omega}_y + I_{yz}\dot{\omega}_z - \left(I_{zz} - I_{xx}\right)\omega_x\omega_z - I_{xz}\left(\omega_x^2 - \omega_z^2\right) - \omega_y\left(\omega_x I_{yz} - \omega_z I_{xy}\right) \tag{83} $$

$$ M_z = I_{zx}\dot{\omega}_x + I_{zy}\dot{\omega}_y + I_{zz}\dot{\omega}_z - \left(I_{xx} - I_{yy}\right)\omega_x\omega_y - I_{xy}\left(\omega_y^2 - \omega_x^2\right) - \omega_z\left(\omega_y I_{xz} - \omega_x I_{yz}\right) \tag{84} $$

If we assume the orientation of the rim such that $I_{ij} = 0$ when $i \neq j$, the rim coordinate system becomes a principal coordinate frame and the moment vector components are identified as:

$$ M_x = I_{xx}\dot{\omega}_x - \left(I_{yy} - I_{zz}\right)\omega_y\omega_z \tag{85} $$

$$ M_y = I_{yy}\dot{\omega}_y - \left(I_{zz} - I_{xx}\right)\omega_x\omega_z \tag{86} $$

$$ M_z = I_{zz}\dot{\omega}_z - \left(I_{xx} - I_{yy}\right)\omega_x\omega_y \tag{87} $$

Consequently:

$$ \ddot{\alpha} = \frac{1}{I_{xx}}\left(M_x + \left(I_{yy} - I_{zz}\right)\dot{\beta}\,\dot{\delta} \right) \tag{88} $$

$$\ddot{\beta} = \frac{1}{I_{yy}}\left(M_y + \left(I_{zz} - I_{xx}\right)\dot{\alpha}\,\dot{\delta} \right) \tag{89}$$

$$\ddot{\delta} = \frac{1}{I_{zz}}\left(M_z + \left(I_{xx} - I_{yy}\right)\dot{\beta}\,\dot{\alpha} \right) \tag{90}$$

The equations for the sidewall moments that exist between the belts segments and the rim are expressed in the wheel local reference frame. In order to express these equations in the global reference frame, the following transformation matrix is used:

$$_{rim}R(t) = R_{Z,\delta(t)}R_{X,\alpha(t)}R_{Z,\beta(t)} \tag{91}$$

It should be noted that the transformation matrix in (91) is a function of time, and is recalculated at every time step based on the spatial orientation of the rim. The final moment vector at the spindle form the tire sidewall, expressed in global reference frame is calculated as:

$$_{sidewall}^{G}M^{i} = {}_{rim}R(t)\cdot {}_{sidewall}^{B}M^{i} \tag{92}$$

Where $_{sidewall}^{B}M$ is the sum of individual torque vectors applied by the belt segments to the tire:

$$_{spindle}^{B}M = \sum_{i=1}^{N_{belt\_seg}}\left({}_{sidewall}^{B}M^{i} \right) \tag{93}$$

5 Tire model parameterization

The tire model parameterization is defined as the set of experiments and data processing methods that are performed to acquire the input parameters for the tire model simulation. There are different methods that can be used for tire parameterization. These methods range from completely empirical to semi-empirical methods. For the model developed in this study a complete set of tire parameterization methods for individual parameters is proposed. In Figure 4, the types of parameters that can be obtained from each set of tests are shown.

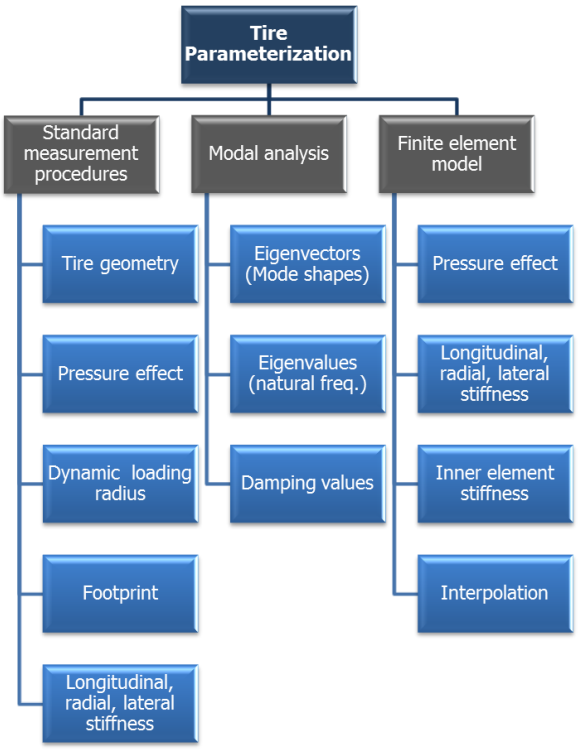

Figure. 4 - Tire parameterization procedures which are used for defining the tire model parameters (gray rectangles), and tire parameters resulted from post-processing of each set of tests (light blue rectangles).

In the tire model developed in this study, the stiffness and the damping characteristics of the tire are considered to be different for in-plane and out-of-plane directions. As a result, during the loading of the tire in the vertical direction, for example, the slope of the tangent line to the loading-deflection curve is not just due to the in-plane radial stiffness of the tire. Therefore, for measuring different stiffness and damping parameters of the model, depending solely on standard measurement procedures is not always effective. Furthermore, conducting a wide variety of tests on the tire in different configuration, such as axial and tangential loading, tire relaxation time measurements, and cleat tests requires a large amount of time and resources, which may not always feasible.

Having these limitations in mind, a finite element model (FEM) of the tire has been implemented [14, 15], which can be used for simulating virtual parameterization tests, as well as for the validation of the lumped mass soft-soil tire model simulations. As mentioned previously, the tire tread is not considered in the initial version of the FEM model to make the validation of the lumped mass model easier. Some material properties of the FEM model were obtained from the manufacturer documentation; the rest of the required properties were obtained through experimental tests done on a similar tire by other researchers [24]. The FEM model validation based on Tire Model Performance Test (TMPT) data is done qualitatively and quantitatively. The details of the TMPT program will be explained in the

"Experimental study" section. In the qualitative method, the trend of the data with different parameter changes is studied. The quantitative approach compares measured data from two similar simulations done with different methods. The finite element model is initially compared with steady-state experimental data. In this regard, the modal analysis test is performed in order to extract tire mode shapes and associated natural frequency and damping values. The schematic of the test rig which is used for conducting the modal analysis experiments on the tire is illustrated in Figure 5.

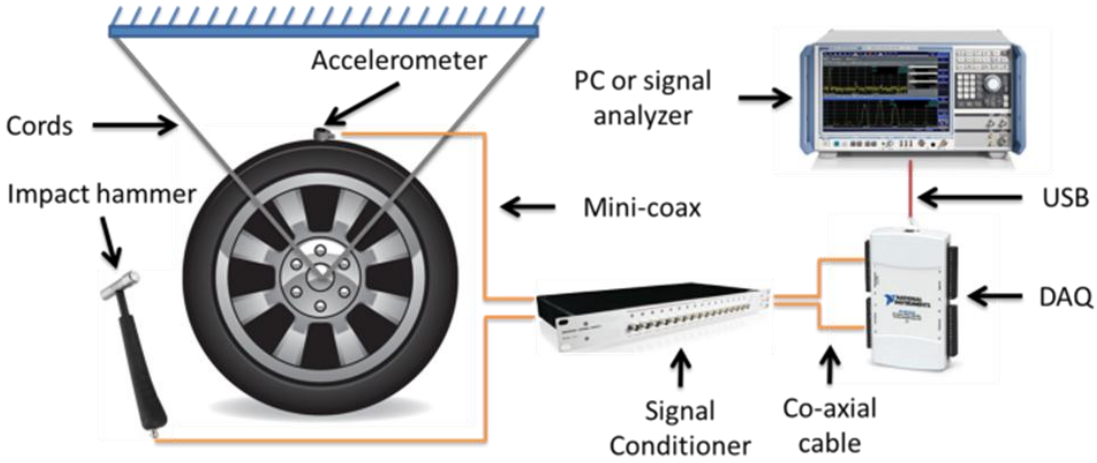

Figure. 5 - The modal analysis test rig used for extracting the tire natural frequencies and damping values. These values are used accordingly to parameterize the tire material model.

The natural frequencies and damping values for the radial modes (R) and transverse modes (T) of the unloaded, non-rotating tire are compared to the experimental values obtained from the TMPT data. The results are shown in Table 1.

Table 1. Comparison between modal analysis simulation test results and experimental data.

	Natural Freq. (Hz)			**Damping %**		
Modes	ABAQUS	Test	Error	ABAQUS	Test	Error
T0	47.54	47.20	0.72	0.023	0.021	9.52
T1	55.85	61.40	9.04	0.031	0.029	6.9
R0	79.35	81.77	2.96	0.066	0.068	2.94
R1	87.60	97.35	10.01	0.041	0.044	6.82
T2	104.68	116.02	9.77	0.038	0.036	5.56
R2	124.74	122.93	1.47	0.027	0.032	15.63
R3	145.17	149.47	2.87	0.02	0.024	16.67
R4	165.48	176.64	6.31	0.021	0.024	12.5

It can be seen that in most of the modes, the FEM model results correlate with the experimental data within a reasonable error margin. Meanwhile, the model slightly underestimates most of the natural frequencies and radial damping values; on the other hand, it overestimates the transverse damping values. The natural frequencies and damping values are further processed in order to find the force elements, stiffness and damping values in different directions (lateral, radial, longitudinal, inner element, etc.).

Additionally, the dynamic loading radius of the tire is measured using the optical distance measuring sensors implemented inside the tire. Footprint of the tire on a flat rough surface is measured through pressure pads, and the stiffness of the tire in radial direction is obtained from tests for which the tire is loaded using hydraulic shakers and vertical reaction forces are measured through the force hub at the tire spindle in the Terramechanics rig [40]. The configuration of the test rig and the design of experiment procedures are presented in a separate publication [41].

6 Tire-terrain interaction

Once the tire structure and tire material properties are modeled and implemented in a mathematical framework, the interface between the model and road surface should be established. This interface searches for the nodal points that are close to the ground (contact search algorithm), and once the contact is detected the algorithm applies the required contact condition (contact interface algorithm). The detailed description of the tire-terrain interaction model is outside the scope of this paper, and is presented in the companion paper [5].

7 Results and discussion

In this section initially we start with a benchmark simulation that demonstrate the dynamic capabilities of the HSSTM model. As it was explained in the tire-terrain interaction section, when the tire is traveling over the terrain, the ground under the contact patch gets deformed. If, for the second time, another tire travels on the same path, it will experience a different amount of resistance from the ground. Furthermore, the elastic and plastic deformation of the terrain would differ during loading and unloading. To visualize this behavior, the deformation of the ground (sandy loam) after two consecutive tire passes is illustrated in Figure 6.

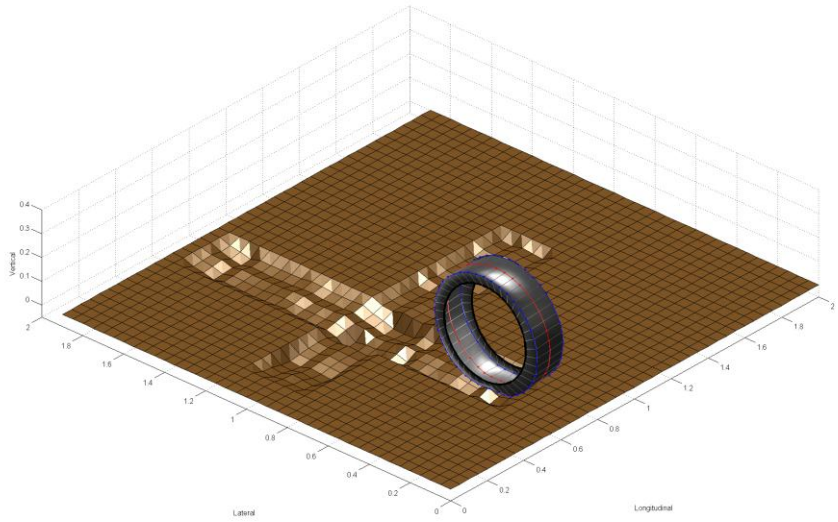

Figure. 6 - Simulation visualization for the multi-pass effect of a sandy loam terrain.

In this simulation, the tire starts traveling over the terrain in a straight line, and deforms the terrain surface, creating a rut. Next, the tire continues on a second path, which is perpendicular to the first path. Because the HSSTM is a nonlinear system, the tire elements go under different states of normal and tangential stresses. As a result, the permanent plastic deformation of the ground after the tire passage is uneven. This deformation has larger value at the crossing section of two paths, which has gone through deformation twice. However, this deformation is less than twice the value of the rut depth on the soil sections negotiated over only once. The mechanical properties of the mineral terrain which is used for conducting this simulation is same as the Medium terrain shown in Table 2.

When the tire is moving on a deformable terrain under an applied torque at its spindle, the positive shear forces keep pushing the tire forward, while the negative ground forces (rolling resistance, bulldozing force, etc.) resist the tire motion. The resultant force is called the drawbar pull, which is an indication for the ability of a vehicle to pull/push external load, accelerate, or overcome the grade resistance. Consequently, in calculation of the drawbar pull, both motion resistance due to tire flexing and the one due to soil compaction are included. To normalize this parameter, it is divided by the normal load at the spindle, thus obtaining the drawbar pull coefficient. The drawbar pull coefficient explicitly relates the tire tractive performance to the wheel slip ratio and implicitly to the terrain normal and shearing characteristics. Using the developed model, the drawbar pull coefficient is calculated at four slip ratio values and on three selective terrain types, which are called soft, medium, and hard soils. The slip ratio is calculated by normalizing the wheel slip velocity with the carriage longitudinal velocity:

$$\kappa = \frac{{}_{wheel}V_{sx}}{{}_{carriage}V_x} \times 100 = \frac{\left(R_{eff}\Omega - {}_{carriage}V_x\right)}{{}_{carriage}V_x} \times 100 \quad (94)$$

Where R_{eff} is the wheel effective rolling radius and Ω is the wheel rotational velocity. The slip ratio values are maintained at their nominal values using a PID controller that regulates the applied torque to the spindle. The terrain mechanical properties used for the simulated terrains are documented in Table 2.

TABLE 2 – Mechanical properties of three mineral terrains used for simulations.

Soil Type	Bekker's equation			Moisture content (%)	Shear characteristics			
	n (–)	K_c $\left(\frac{kN}{m^{n+1}}\right)$	K_ϕ $\left(\frac{kN}{m^{n+1}}\right)$		RS $\left(\frac{cm}{s}\right)$	C $\left(\frac{kN}{m^{n+1}}\right)$	Φ (deg)	K (–)
Soft terrain (LETE soil)	0.611	1.16	475.0	0	2.5	1.15	31.5	-
Medium terrain (Upland sandy loam)	0.74	26.8	1522	44.3	2.5	2.7	26.1	0.45
Hard soil (Grenville loam)	1.01	0.06	5880	24.1	2.5	3.1	29.8	0.40

The results of this simulation that indicate the effect of the terrain properties on the mobility performance of the tire are presented in the Figure 7.

It was observed that increasing the stiffness of the terrain could increase the peak of the drawbar pull coefficient in addition to its asymptotic value at high slip ratios. The difference between the drawbar pull coefficient on the hard and medium soils decreases drastically with increasing the slip ratio. This is expected to be a direct effect of the K parameter variations. As it was discussed earlier, K is the shear deformation parameter and is a measurement of the magnitude of the shear displacement required for developing the maximum shear stress in the soil. The low slip ratio region is highly affected by the shear deformation parameter K, whereas the high slip ratio region is almost insensitive to the its variations [42]. Therefore, the hard soil, with a lower K value, shows higher drawbar pull coefficients at low slip values, and the difference attenuates by approaching the high slip ratio region. An analogous trend for the drawbar pull values measured on the similar terrains was reported by other researchers [26].

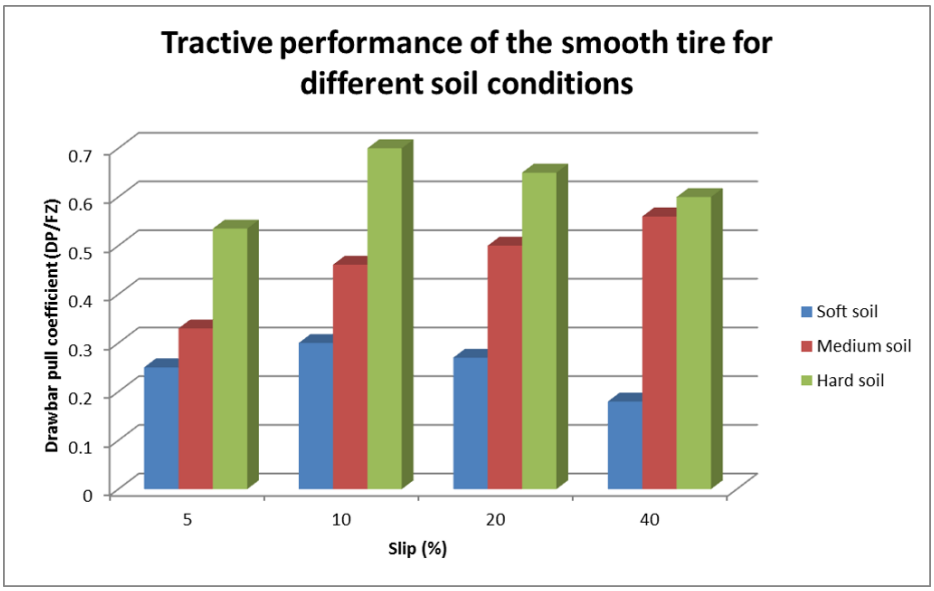

Figure. 7 - Tractive performance of the buffed tire simulated at four slip ratios and three different soil conditions.

In order to characterize the configuration of the test rig in the simulation environment, an application platform is designed in order to accommodate the communications with the multibody dynamics solver. The spindle carriage is represented using a quarter car model, and is implemented in a separate module, which has its own ODE solver. At every time step, the vehicle model, which is described in a multibody dynamics framework, provides the wheel kinetics and kinematics variables to the tire model. The time step for the tire model solver is chosen as half the time step set for the multibody dynamics solver. This is due to the fact that extra calculations are performed in the middle of the fixed time intervals to improve the accuracy. These extra calculation results are provided to the external solver for maximizing the ODE solver performance. Next, the tire model updates the position and velocity state vectors of the tire. Using this new tire configuration, the terrain model exploits the contact conditions, which results in the tire/ground deflection and stress distribution in the contact patch. The normal and shear stress fields are feedback to the tire model, which are used for solving the tire equations of motion. At the end of this step, the tire model calculates three forces and moments at the spindle and feeds them back to the vehicle model. An overview of the discussed procedure is shown in Figure 8. It should be noted that a great attention is given to the optimization of the tire model performance in order to make it a practical option for full vehicle simulations. This has become possible by applying some parallelization and multi-processing techniques to the architecture of the program. Additionally, as for the tire-vehicle interface, the data communication routines are developed such that they follow the standard formats from Standard Tire Interface (STI) practices.

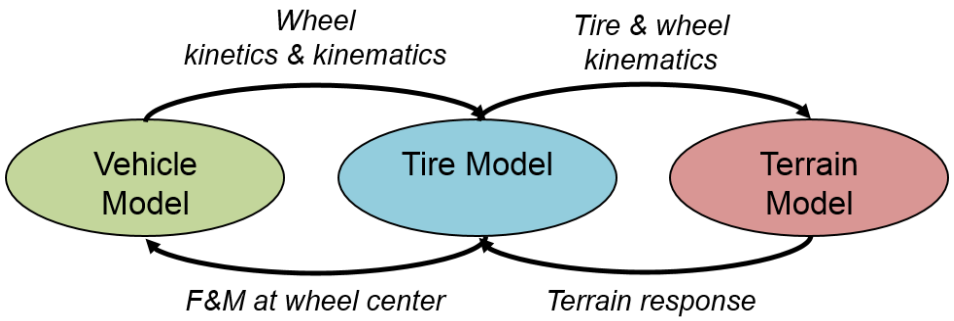

Figure. 8 - The communication data flow between the tire model modules during the full vehicle simulation.

The vehicle handling and rollover behavior are directly affected by the force and moments at the wheel spindle. In this regard, the longitudinal force, the lateral force, and the aligning moment values are the quantities of interest because they define the planar motion of the vehicle. In order to validate the developed model based on these system response quantities, a straight line driving maneuver is designed. In this test, the tire carriage is moved with the constant longitudinal speed of 0.5 m/s while a normal force of 4,000 N is maintained at the spindle. Meanwhile, the applied driving torque at the spindle is increased with a constant rate to allow the wheel slip ratio changes from 0 % to 60 %. All the forces and moments are measured at the spindle, and the wheel sinkage is calculated using a novel method developed by Naranjo [33]. In this method, the wheel sinkage is calculated by post-processing the data from the sensors that are implemented inside the tire cavity. These sensors are integrated units composed of a position sensitive detector (PSD), five infrared emitting diodes (IREDs), and a signal processing circuit. The similar test configuration is designed using the developed tire model platform, and simulation runs are conducted at the input conditions identical to the experimental test setup. The tire used for conducting the tests is a P225/60R16 97S Radial Reference Test Tire from Michelin. The tire tread is buffed in order to study the performance of the treadles tire.

The validation of the tire model response quantities versus the measurement data is done using the cross plot validation charts. For every parameter, simulation results are plotted versus the test data across the entire simulation time span. Next, a linear line is curve-fitted to the resulted data points, and is plotted on the same figure. The validation results for four main response quantities, including sinkage, longitudinal force, lateral force, and aligning moment are shown in Figures 9 to 12. The ideal case would be for all the data points to line up on the green curve-fitted line and for this line to match the 1:1 red dash line. However, due to errors such as measurement errors, modeling errors, and parameterization errors, this ideal situation is almost impossible to achieve. To assess the quality of the match, curve-fitted line properties including the slope, intersection with the Y axis and coefficient of determination (R^2) are shown

on the figures. For a perfect match, two main parameters of interest, which are the line slope and the R^2 index would be equal to one. The R^2 index is an indication of how the data is distributed around the curve-fitted line; so, for a completely scattered data, this value will become zero.

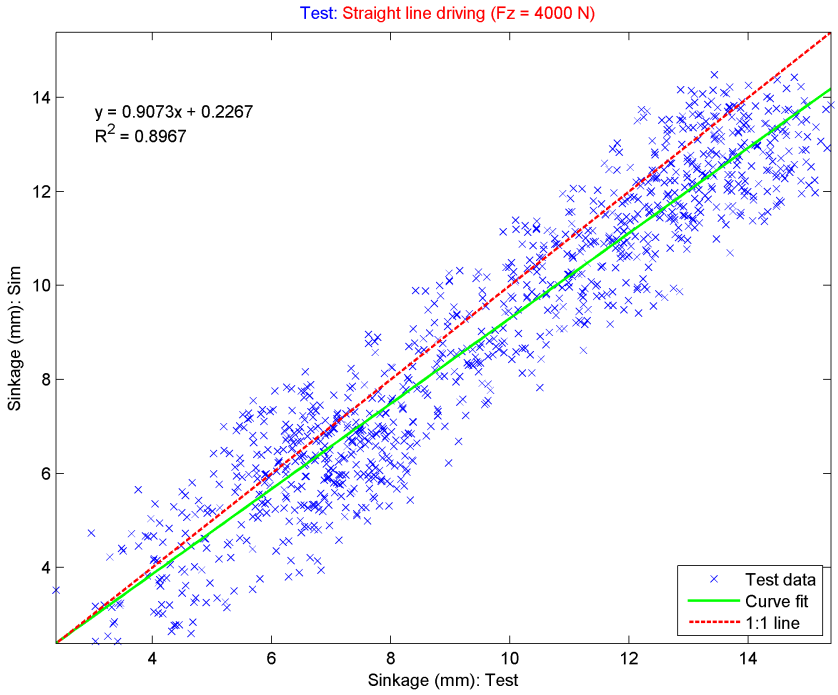

Figure. 9 - System response quantities cross-plot validation: wheel sinkage

Looking at the sinkage and the longitudinal force validation plots suggests that the HSSTM model can do a good job in estimating these parameters. The solid green curve-fitted line in the sinkage plot starts to deviate from the 1:1 line as the sinkage increases, and always remains below the red dashed line. This means that at higher sinkage values, the measured sinkage value is greater than the simulation results. The higher sinkage values occur at higher slip values, at which the tire starts to displace large volumes of soil particles and dig into the terrain. Considering the fact that the soil volume displacement model is not used in this simulation can justify the trend of the sinkage cross-plot results. As for the longitudinal force, the model represent a good performance in estimating the measurement data.

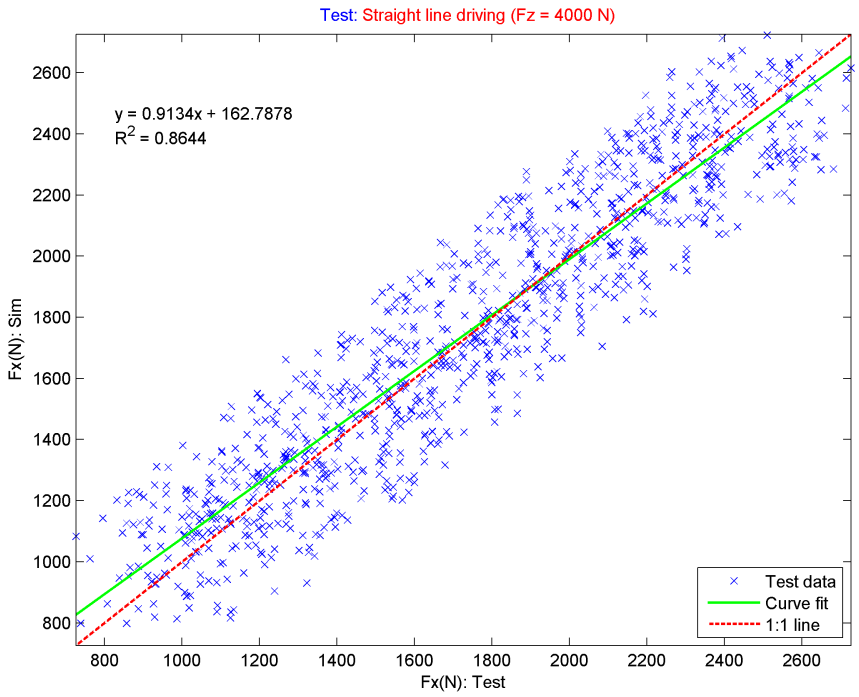

Figure. 10 - System response quantities cross-plot validation: longitudinal force at the spindle

As shown in Figures 11 and 12, although the test runs are performed in a straight line, the lateral force and the aligning moment values change during these maneuvers. This can be explained by considering the following facts: (1) when the tire is traveling on a solid, non-deformable ground, it produces a lateral force and an aligning moment. This results from the plysteer and the conicity in the tire construction. The effect of these manufacturing defects is modeled as a pseudo slip angle (for plysteer) and a pseudo inclination angle (for conicity). The pseudo slip angle and the inclination angle (camber angle) cause the residual lateral force and aligning moment to appear in the straight line maneuvers; (2) The ground surface is not fully flat and does not have identical mechanical properties in all directions (non-isotropic). Therefore, once the tire deforms the terrain, the ground reaction force would not be parallel to the wheel direction of motion. This inclined reaction force produces a component perpendicular to the wheel plane. Additionally, when the tire sinks into the ground, soil pressure distribution is applied to the tire sidewalls from the accumulated soil pile that is displaced out of the tire path. This force is known as bulldozing force, and contributes to the lateral force and, consequently, to the aligning moment generation. The wheel carriage in the Terramechanics test rig is located near the right wall of the experimental test rig. Therefore, the soil is piled up near the wall edges, and produces a pressure gradient on the tire sidewall that shifts the generated lateral force values. This effect can be observed in the shape of the lateral force cross-plot data points. As shown in Figure 11, most of the blue data points

are speeded below the green solid curve-fitted line, which means that model underestimates the lateral force values throughout the simulation.

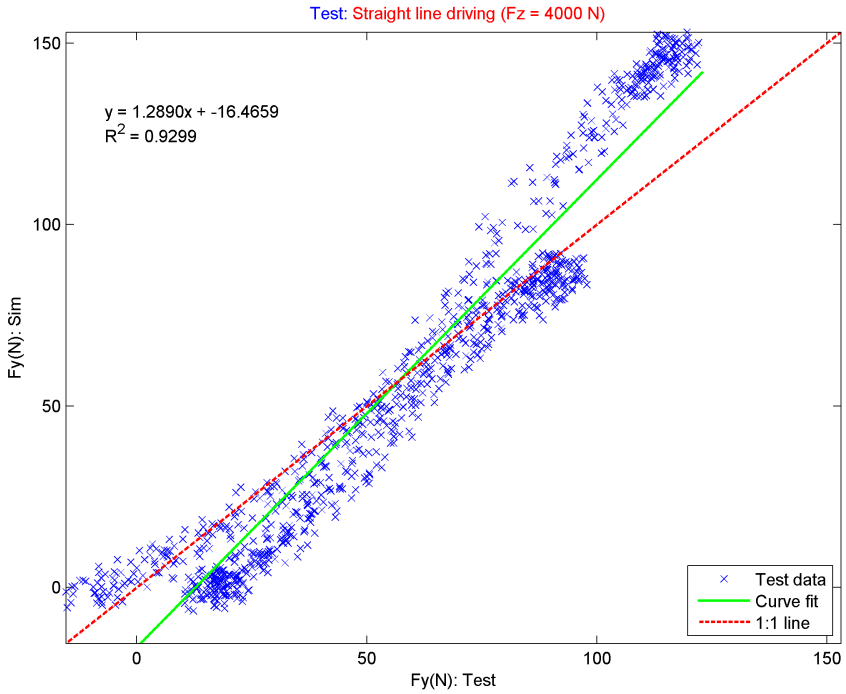

Figure. 11 - System response quantities cross-plot validation: lateral force at the spindle

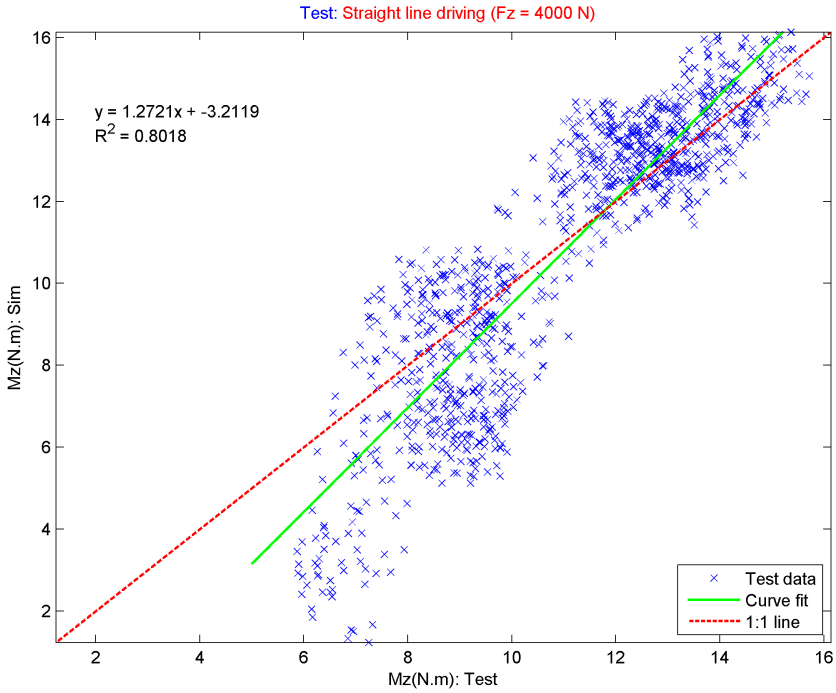

FIG. 12 - System response quantities cross-plot validation: aligning moment at the spindle

8 Conclusion

In order to model the dynamic behavior of the tire on soft soil, a lumped mass discretized tire model using Kelvin-Voigt elements is developed. This model, named HSSTM, is developed to be easily linked with multibody dynamics software packages to simulate vehicle performance on deformable terrains. To optimize the computational time of the code, different techniques were used in memory allocation, parameter initialization, code sequence, and multi-processing. The computational time of the code had a significant improvement relative to previous codes developed in this institute up to the speed of real time simulations.

The tire parameterization is performed using a reduced finite element tire model for the same tire, modal analysis, and other experimental test procedures. In the parameterization step sensitivity analysis tools were incorporated in order to reduce the complexity of the model, and fit more accurate parameters values based on the test data.

Experimental tests were performed on the Terramechanics rig at the Advanced Vehicle Dynamics Laboratory at Virginia Tech using the P225/60R16 97S Radial Reference Test Tire from Michelin. The tests were performed on sandy loam, and data were collected for various case studies and parameter changes.

Different case studies were simulated in order to analyze the performance of the developed model. Initially, a soil multi-pass effect simulation is conducted to demonstrate the functionality of the model. Next, the tire drawbar pull coefficients on three selective terrains are estimated. It is shown that the drawbar pull coefficients are mainly influenced by the terrain stiffness and shear deformation parameter. As for the validation case studies, a straight line driving maneuver is conducted at constant normal load and varying slip ratio values. Using the cross-plot validation graphs it is shown that the HSSTM can estimate four main vehicle handling parameters including longitudinal force, lateral force, aligning moment, and sinkage with a reasonable accuracy. The observed discrepancies are thought to be mainly from the test conditions that are not modeled in the simulations, such as soil displacement at high slip ratios, tire construction defects (plysteer, comity), and soil bulldozing effect due to the soil compaction near the walls of the test rig.

9 Acknowledgment

This project is funded in part by the Automotive Research Center, a U.S. Army Center of Excellence for Modeling and Simulation of Ground Vehicles. We want to thank our quad members, Dr. B. Ross from Motion Port and Mr. D. Christ from Michelin for all of the time and support they have dedicated to us.

10 References

1. Gipser, M., *The FTire Tire Model Family*. 2003, Esslingen University of Applied Sciences: Esslingen, Germany. p. 18.
2. Oertel, C., *On Modeling Contact and Friction Calculation of Tyre Response on Uneven Roads.* Vehicle System Dynamics, 1997. **27**(S1): p. 289-302.
3. Oertel, C. and A. Fandre. *Ride Comfort Simulations and Steps Towards Life Time Calculations: RMOD-K and ADAMS*. in *International ADAMS User's Conference*. 1999. Berlin, Germany.
4. Gallrein, A. and M. Backer, *CDTire: A tire model for comfort and durability applications.* Vehicle System Dynamics, 2007. **45**(1): p. 69-77.
5. Taheri, S., C. Sandu, and S. Taheri, *Hybrid Soft Soil Tire Model (HSSTM). Part II: Tire-Terrain Interaction Modeling.* Journal of Terramechanics, 2015.
6. Taheri, S., et al., *A technical survey on Terramechanics models for tire–terrain interaction used in modeling and simulation of wheeled vehicles.* Journal of Terramechanics, 2015. **57**: p. 1-22.
7. Pacejka, H.B., and Bakker, E., *The Magic Formula Tyre Model.* Vehicle System Dynamics, 1992. **21**(001): p. 1-18.
8. Pacejka, H.B. and E. Bakker, *The Magic Formula Tyre Model.* Vehicle System Dynamics, 1992. **21**(001): p. 1-18.
9. Chae, S., *Nonlinear Finite Element Modeling and Analysis of a Truck Tire*, in *Intercollege Graduate Program in Materials*. 2006, Pennsylvania State University. p. 207.
10. Mastinu, G. and E. Pairana, *Parameter Identification and Validation of a Pneumatic Tyre Model.* Vehicle System Dynamics, 1992. **21**(01): p. 58-81.
11. Kilner, J., *Pneumatic tire model for aircraft simulation.* Journal of Aircraft, 1982. **19**(10): p. 851-857.
12. Madsen, J., et al., *A Physics-Based Vehicle/Terrain Interaction Model for Soft Soil Off-Road Vehicle Simulations.* SAE International Journal of Commercial Vehicles, 2012. **5**(1): p. 280-290.
13. Negrut, D. and J.S. Freeman, *Dynamic tire modeling for application with vehicle simulations incorporating terrain.* SAE transactions, 1994. **103**(6): p. 96-103.
14. Taheri, S., *Finite Element Modeling of Tire-Terrain Dynamic Interaction for Full Vehicle Simulation Application* in *Mechanical Engineering* 2014, Virginia Tech Blacksburg, Virginia
15. Taheri, S., C. Sandu, and S. Taheri, *Finite Element Modeling of Tire Transient Characteristics in Dynamic Maneuvers.* SAE international Journal of Passenger Cars, 2014. **7**(1): p. 9.
16. Chan, B.J., *Development of an off-road capable tire model for vehicle dynamics simulations*, in *Mechanical Engineering*. 2008, Virginia Tech: Blacksburg, VA. p. 226.
17. Chan, B.J. and C. Sandu, *Development of a 3-D Quasi-static Tire Model for On-road and Off-road Vehicle Dynamics Simulations: Part III–Off-road Flexible Wheel Model.* International Journal of Vehicle Systems Modelling and Testing, 2014. **9**(2): p. 151-176.
18. Chan, B.J. and C. Sandu, *Development of a 3-D Quasi-static Tire Model for On-road and Off-road Vehicle Dynamics Simulations: Part II–Off-road Rigid Wheel Model.* International Journal of Vehicle Systems Modelling and Testing, May 2014. **9**(2): p. 107-136.
19. Chan, B.J. and C. Sandu, *Development of a 3-D Quasi-static Tire Model for On-road and Off-road Vehicle Dynamics Simulations: Part I–On-road Flexible Tire Model.* International Journal of Vehicle Systems Modelling and Testing, 2014. **9**(1): p. 77-105

20. Wong, J.Y. and V.M. Asnani, *Study of the correlation between the performances of lunar vehicle wheels predicted by the Nepean wheeled vehicle performance model and test data.* Proceedings of the Institution of Mechanical Engineers, Part D: Journal of Automobile Engineering, 2008. **222**(11): p. 1939-1954.
21. Bekker, M.G., *Introduction to Terrain-Vehicle System*. 1969: Ann Arbor: The University of Michigan Press.
22. Bekker, M.G., *Off the Road Locomotion*. 1960, Ann Arbor, Michigan: University of Michigan Press.
23. Bekker, M.G., *The Theory of Land Locomotion*. 1956, Ann Arbor, Michigan: University of Michigan Press.
24. Bekker, M.G., *Theory of Land Locomotion : The Mechanics of Vehicle Mobility*. 1956: Ann Arbor: The University of Michigan Press.
25. Wong, J.Y. and J. Preston-Thomas, *On the Characterization of the Shear Stress-Displacement Relationship of Terrain.* Journal of Terramechanics, 1983. **19**(4): p. 225-234.
26. Wong, J.Y., *On The Study of Wheel-Soil Interaction.* Journal of Terramechanics, 1984. **21**(2): p. 117-131.
27. Wong, J.Y. and A.R. Reece, *Prediction of Rigid Wheel Performance Based on the Analysis of Soil-Wheel Stresses. Part I. Performance of Driven Rigid Wheels.* Journal of Terramechanics, 1967. **4**(1): p. 81-98.
28. Wong, J.Y. and A.R. Reece, *Prediction of Rigid Wheel Performance Based on the Analysis of Soil-Wheel Stresses. Part II. Performance of Towed Rigid Wheels.* Journal of Terramechanics, 1967. **4**(2): p. 7-25.
29. Teheri, S., et al. *Off-road Soft Soil Tire Model*. in *Presentation for the 7th Americas Regional ISTVS Conference* 2013. Tampa, FL.
30. Taheri, S., C. Sandu, and S. Taheri. *Development and Implementation of a Hybrid Soft Soil Tire Model (HSSTM)*. in *The 18th International ISTVS Conference Seoul, Korea.* 2014.
31. Pinto, E., *A Three Dimensional Discretized Tire Model for Soft Soil Applications*, in *Mechanical Engineering*. 2012, Virginia Tech: Blacksburg, VA.
32. Sandu, C., et al. *Off-Road Soft Soil Tire Model and Experimental Testing*. in *Proceedings of the 12th European ISTVS Conference* 2012. Pretoria, South Africa.
33. Sandu, C., et al. *Off-Road Soft Soil Tire Model Development, Validation, and Interface to Commercial Multibody Dynamics Software*. in *Proceedings of the 17th International ISTVS Conference* 2011. Blacksburg, VA, USA.
34. Umsrithong, A. and C. Sandu, *A 3D semi-empirical on-road transient tire model.* SAE International Journal of Commercial Vehicles, 2010. **3**(1): p. 42-59.
35. Umsrithong, A. and C. Sandu. *A 3D semi-empirical stochastic tire model on hard flat and uneven surfaces*. in *International Congress on Automotive and Transport Engineering*. 2010. Brasov, Romania.
36. Umsrithong, A., *Deterministic and Stochastic Semi-Empirical Transient Tire Models*. 2012, Virginia Tech: Blacksburg, VA.
37. Umsrithong, A. and C. Sandu. *Parameter Identification and Experimental Validation of a Discrete Mass Tire Model for Uneven Rigid Terrain*. in *Proceedings of ASME 2012 IDETC/CIE 14th International Conference on Advance Vehicle Technologies (AVT)*. 2012. Chicago, IL: American Society of Mechanical Engineers.
38. Umsrithong, A. and C. Sandu, *A Semi-Empirical Tire Model for Transient Maneuver of On Road Vehicle*, in *SAE Commercial Vehicle Engineering Congress and Exposition*. 2009: Chicago, IL. p. 9.
39. Umsrithong, A. and C. Sandu, *Stochastic transient tyre model for vehicle dynamic simulations on rough rigid ground.* International Journal of Vehicle Systems Modelling and Testing, 2012. **7**(4): p. 351-371.
40. Dasch, J.M. and D.J. Gorsich, *TARDEC Story: Sixty-Five Years of Innovation, 1846-2010*. 2012: Defense Department, Army, U.S. Army Tank Automotive Research, Development and Engineering Center (TARDEC).
41. Naranjo, S.D., et al., *Experimental testing of an off-road instrumented tire on soft soil.* Journal of Terramechanics, 2014. **56**: p. 119-137.
42. Wong, J.Y., *Terramechanics and Off-Road Vehicle Engineering: Terrain Behaviour, Off-Road Vehicle Performance and Design*. 2nd Edition ed. 2010, Amsterdam, The Netherlands: Elsevier.